Geotechnical Engineering

Pre-stressing of soil and structures due to jet grouting
Rabaiotti, Malecki, Amstad and Puzrin

ice | proceedings

Proceedings of the Institution of Civil Engineers

http://dx.doi.org/10.1680/geng.14.00112
Paper 1400112
Received 07/07/2014 Accepted 07/11/2014
Keywords: diaphragm walls/field testing & monitoring/grouting

ice Institution of Civil Engineers publishing

Pre-stressing of soil and structures due to jet grouting

1 **Carlo Rabaiotti** Dr Sc
Project Leader, Basler & Hofmann AG, Esslingen, Switzerland; also Senior Lecturer, ETH Zürich, Switzerland

2 **Cornelia Malecki** MSc
Project Engineer, Basler & Hofmann AG, Esslingen, Switzerland

3 **Mathias Amstad** MSc
Research Assistant, Institute for Geotechnical Engineering, ETH Zürich, Zürich, Switzerland

4 **Alexander M. Puzrin** FICE
Professor Dr, Institute for Geotechnical Engineering, ETH Zürich, Zürich, Switzerland

Jet grouting is a widely used technique for soil stabilisation, which provides support to geotechnical structures and buildings. One of the main problems related to this technique is excessive displacement and occasionally high pressures induced on structures in direct contact with the jetted area. This paper studies another possible problem caused by jet grouting: the excessive pre-stressing of retaining walls and soil in an excavation pit and the subsequent pressure release to the retaining structural elements, the steel struts, during and after excavation. In the example described here, the construction of a deep jet grouting slab, equivalent to a soil-embedded strut, induced stresses in the soil and in the diaphragm walls of a test shaft. The stresses were released to the steel struts during the subsequent excavation. These additional stresses could potentially exceed the design loads and, in the worst-case scenario, lead to failure. In this case study, the forces released to the struts after the excavation were 2·5 times higher than those predicted by considering only earth pressure without introducing the pre-stressing induced by the jet grouting. Thanks to application of the observational method and adequate risk management strategy, no failure occurred.

Notation

C_c	coefficient of primary compression
C_s	coefficient of secondary compression
d	layer thickness
d_{tot}	thickness of the geotechnical unit
E	Young's modulus of elasticity
M_E	confined stiffness modulus
M_{Eh}	horizontal confined stiffness modulus
M_{Ev}	vertical confined stiffness modulus
q	deviatoric stress
S_u	undrained shear strength
u	horizontal wall or soil displacement
γ_s	deviatoric strain
ζ	standard deviation
λ	logarithmic mean
μ	physical mean value
σ_c	compressive strength
σ_t	tensile strength
σ'_z	vertical effective earth pressure
σ'_1	maximum principal stress
σ'_3	minimum principal stress

1. Introduction

Jet grouting is an extremely versatile technique for stabilising soil. It was developed in the 1950s in England and Japan and since then has experienced success worldwide in a wide spectrum of applications: for instance in underpinning foundations, stabilising retaining walls and sealing dams. The process consists of injecting and mixing cement into the soil mass. The cement is injected through a rotating nozzle at high pressure. The soil is eroded and mixed with the cement suspension, creating a column of cement-stabilised material. Three main techniques are in use today: cement-only suspension (single fluid); combined with air (double fluid); and combined with air and water (triple fluid) (Croce *et al.*, 2014).

One well-known possible problem with this technique is deformation in the surrounding soil and adjacent structures, as well as an increase in earth pressure. For example, the effect of different jet grouting methods on neighbouring structures was studied by Wang *et al.* (1999), who measured the displacement of a diaphragm wall induced by the construction of an adjacent soil-embedded jet grouting slab, whose depth was between −11 m and −14 m from ground level. Depending on the jet grouting

technique adopted, a maximum horizontal displacement of 5 to 25 mm was found. The measured increase in the earth pressure values varied from 50 kPa (5 mm displacement) to 150 kPa (25 mm displacement). Similarly, Poh and Wong (2001) carried out a field trial with a jet grouting slab (excavation depth: 10·5 m, slab length: 6·75 m, slab width: 6·4 m and column length: 9 m) in contact with a diaphragm wall in marine clay. They found that the jet grouting induced a bending moment of 156–195 kNm/m in the diaphragm wall, and a maximum increase of 73 kPa in earth pressure in the region next to the grouted area.

More recently, Wang *et al.* (2013) investigated the effects of field installation of horizontal twin-jet grouting in Shanghai soft soil deposits. This new technique consists of injecting a mixture of compressed air, cement and sodium silicate. For a jet grouting slab 11 m deep, realised in soft clay in the centre section of a future tunnel, they measured a maximum lateral subsoil displacement of about 33 mm and a maximum increase of about 40 kPa in earth pressure. After the jet grouting process had ended, the earth pressure and excess pore-water pressure dissipated.

In these examples, which are typical of those in the literature, the emphasis has been on the effects of grouting on surrounding soil and existing structures, rather than on subsequent effects on any retaining system (e.g. struts) used within the jet grouted structure after excavation. Either the pressure induced by the jet grouting was able to dissipate over time, or there was no braced excavation in the area close to the deformed wall. In contrast, in this paper it will be shown that jet grouting slabs adopted as a soil-embedded retaining element in narrow excavations can induce very large forces in rigid retaining systems, which can potentially exceed design loads and lead to failure.

This study is part of a preliminary investigation carried out for a new large underground structure, planned under the existing main railway station in the city of Lucerne, Switzerland. In this context, a test shaft was built and instruments were installed in it in order to study the proposed construction technique, in particular the feasibility of jet grouting as a structural and groundwater sealing element. The geology and hydrology of the site were also studied. Before and during the construction of the shaft, geological in situ and laboratory investigations were carried out: triaxial and oedometer tests (IG TiBLU, 2013) were made on undisturbed soil samples extracted at different depths; flat dilatometer tests (Marchetti dilatometer test (DMT)), cone penetration tests with piezometer (CPTU) and self-boring pressuremeter (SBP) tests were additionally performed inside and outside the excavation pit and on the perimeter of the area where the station will be built.

Although the main topic of this paper is the analysis of particular side effects of jet grouting, the results of the geological investigation are also crucial for understanding the observed phenomena. Therefore Section 2 of this paper is devoted to the soil investigation carried out ahead of construction and to the probabilistic characterisation of the geological properties of the soil. Technical specifications and the construction of the shaft are described in Section 3. In Section 4 it will be shown that the jet grouting process inflated the shaft and pre-stressed its diaphragm walls as well as the surrounding soil. The maximum displacement of the diaphragm walls due to the jet grouting was large (about 13 cm). In addition, strut forces much higher than those predicted from active or even at-rest earth pressure were measured during excavation. By analysing the measured changes in the shape of the shaft, the soil deformation and the forces in the struts, it is possible to determine the strength and stiffness of the geological units as well as the magnitude and the area of influence of the pressure that led to the expansion of the shaft. In particular, the measured soil stiffness and strength obtained from the in situ and laboratory tests are compared with those obtained by back-calculation of the shaft displacements and strut forces.

2. Geology

2.1 Stratigraphy

The soil beneath the main railway station in Lucerne consists of a series of glacial and postglacial soft alluvial strata. Clay, silt, sand and gravel layers due to different sedimentation processes are dominant. In the area of the test shaft, the soil is characterised by at least nine different layers: Figure 1(a) shows the soil stratigraphy for the test shaft based on a soil sample classification (Schwager, 2013). Within the perimeter of the future underground railway station, the thickness, depth and distribution of the different soil layer materials vary considerably. More comprehensive layers made up of heterogeneous material are therefore considered in this study in order to obtain a homogeneous model for the analysis. These are identified by the sedimentation history (Keller (2011); see also Figure 1(a)). The alluvium in the lacustrine basin of Lake Lucerne has developed since the last glacial maximum and reaches a thickness of over 100 m in the area of the railway station. It can be seen in Figures 1(a) and 1(b) that the geotechnical unit D consists of a series of sandy layers that are interrupted by clay-rich deposits. In this paper, the focus is on the characterisation of unit D, which is the most relevant for the design and the behaviour of the test shaft.

2.2 Laboratory tests

The aim of the laboratory tests was to understand the mechanical behaviour of the soil in different loading conditions as well as to obtain reliable parameters for the design of the structural elements of the future underground station and tunnel. The tests were carried out on undisturbed soil samples (IG TiBLU, 2013) obtained from the casings of a hydraulic piston sampler.

2.2.1 Undrained triaxial shear tests

The triaxial tests were carried out under undrained conditions measuring the development of the pore-water pressures in the specimen. Thus, it is possible to obtain undrained and drained soil properties, as the drained properties are calculated from the measured pore-water pressures. Additional studies carried out by Schwager (2013) confirm that the choice to carry out the tests

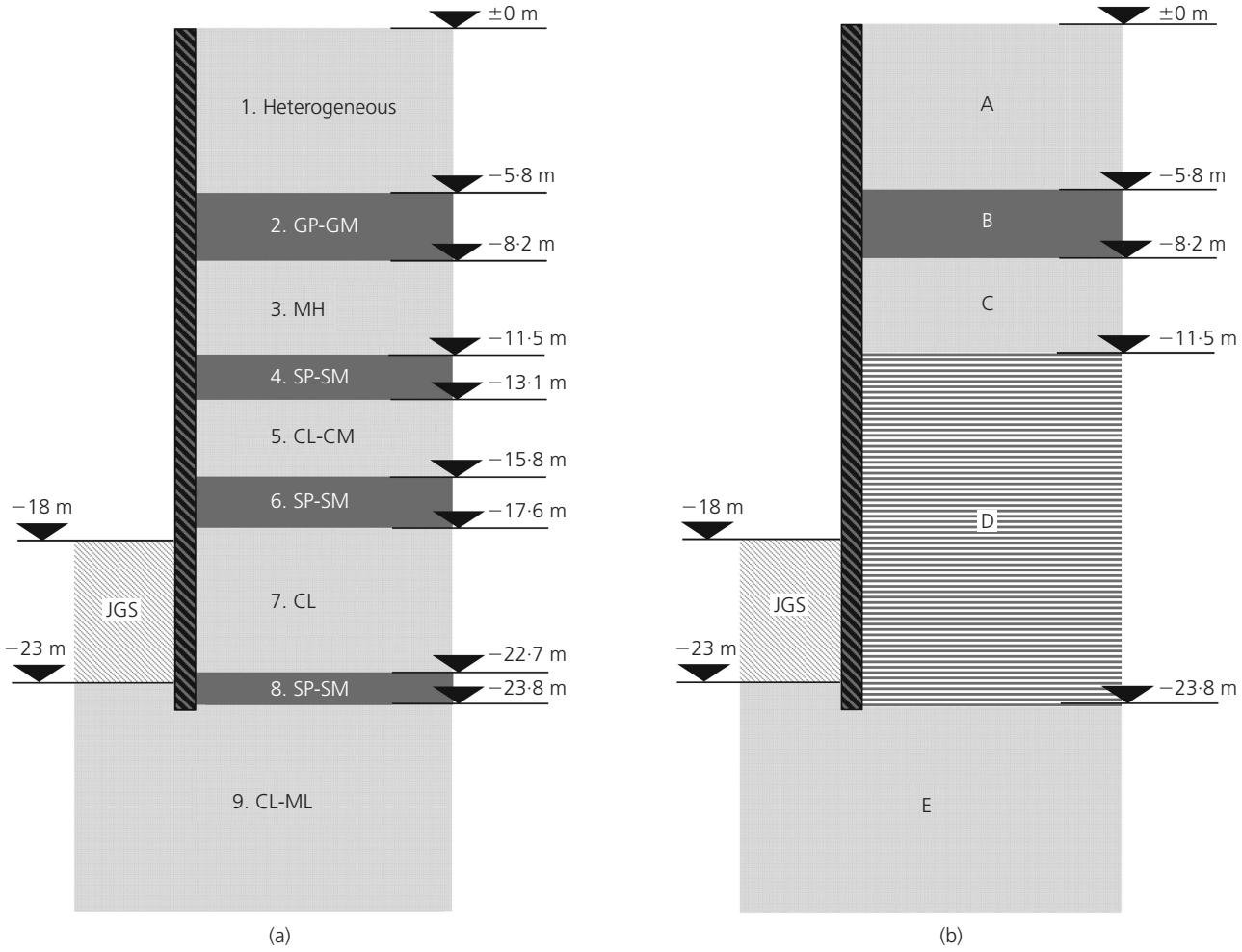

Figure 1. (a) Geological units in project area. The soil type is described according to the unified soil classification system (USCS) classification system. JGS indicates jet grouting slab. (b) Simplified geotechnical soil model with main geotechnical units

under undrained conditions reflects the real in situ soil behaviour during jet grouting and excavation. Table 1 shows the results of the undrained compression and extension tests carried out after anisotropic consolidation. It can be seen that soil properties within a layer are fairly homogeneous, without large anisotropy. Generally, since only the most cohesive part of the core could be extracted intact to enable the specimen to be prepared for the test, the results show higher undrained shear strength than the results from the in situ tests.

2.2.2 Oedometer tests

The results of oedometer tests at different depths and for different layers are shown in Table 2. As can be observed, the soil, mainly silt and low-plasticity clay, is normally consolidated and relatively soft. In the table, the pressure-dependent confined stiffness moduli are also shown. These are to provide a comparison to those back-calculated in the finite-element analysis described in Section 4.

Layer	Soil	Stress path	Preconsolidation pressure		Undrained shear strength
			σ'_1: kPa	σ'_3: kPa	S_u: kPa
3	MH	LE	100	60	42
3	MH	LE	100	60	51
3	MH	LE	100	60	47
5	CM	LE	220	132	55
9	CL-ML	AE	260	156	82
9	CM	LC	260	156	78
9	CM	LC	260	156	78

Table 1. Soil properties from undrained triaxial tests. Anisotropic consolidation (LE: lateral extension; LC: lateral compression; AE: axial extension)

Layer	Classification	Depth: m	C_c	C_s	Overconsolidation ratio (OCR)	σ'_z: kN/m^2	M_E: MN/m^2
3	MH	11·6	0·393	0·038	1·0	117·8	2·7
3	MH	12·1	0·365	0·035	1·0	121·8	2·9
5	CM	16·5	0·314	0·039	1·0	157	3·6
7	CL	20·1	0·144	0·015	1·2	185·8	7·5
9	CL-ML	26·8	0·229	0·045	1·0	239·4	6·0
9	CL-ML	29·0	0·087	0·015	1·2	257	15·2
9	CL-ML	29·3	0·074	0·011	1·3	259·4	16·8
9	CL-ML	29·6	0·100	0·011	1·2	261·8	12·7
9	CL-ML	33·4	0·215	0·030	1·4	292·2	6·6
9	CM	36·5	0·223	0·031	1·0	317	7·5

Table 2. Soil properties from oedometer tests

2.3 In situ tests

The soil conditions at the test shaft were additionally investigated by means of in situ tests. CPTUs were carried out inside the area of the shaft before its construction. DMTs and SBP tests were carried out outside the shaft (see Figure 2).

Figures 3(a) and 3(b) show the confined stiffness modulus and the undrained shear strength obtained with the different in situ measurement devices. For layers with high clay content, the confined stiffness modulus (M_E) values from the oedometer test correspond well with the results of both DMT and CPTU. For the sandy soils, the CPTU values are much higher than those from oedometer testing or DMT. The undrained shear strength (S_u) predicted by CPTU and DMT also corresponds well with the values from the other in situ tests and the triaxial test results. The results from the SBP are very high compared with those measured by the other devices. The difference is due to the lower vertical spatial resolution of the SBP, whose results are much more affected by the influence of the stiff layers.

2.4 Determination of soil parameters for geotechnical units

As already mentioned, it would not be useful for the purposes of this research to obtain soil parameters for single soil layers, whose thicknesses vary considerably within the perimeter of the future underground station. Therefore the geotechnical parameters are derived for the geotechnical units, which have a more uniform thickness over this region.

For the geotechnical units C and E, geotechnical parameters can directly be derived from layers 3 and 9. For unit D, several different soil types need to be considered. Puzrin *et al.* (2010) show that using a mean value for S_u from different soil types may lead to an overestimation of the bearing capacity. For a multi-layer problem, the authors suggest considering only the strength parameters of the weaker layers. Thus, only the strength properties of the softer layers 5 and 7 are taken into account for S_u. For those layers, the distribution of S_u has a coefficient of variation, COV = 0·19. According to Schneider and Schneider (2013), a normal distribution can therefore be used to describe S_u statistically, as is observed in Figure 4.

In contrast, a mean stiffness M_E for the geotechnical unit D may be useful to improve the prediction of deformations of the diaphragm walls and of the soil at serviceability limit states. According to Figure 3(a), the stiff sandy layers 4, 6 and 8 (SP-SM) can be distinguished from the soft layers 5 and 7 (CL or CL-CM). In order to find M_E for unit D, the soil structure is simplified by assuming

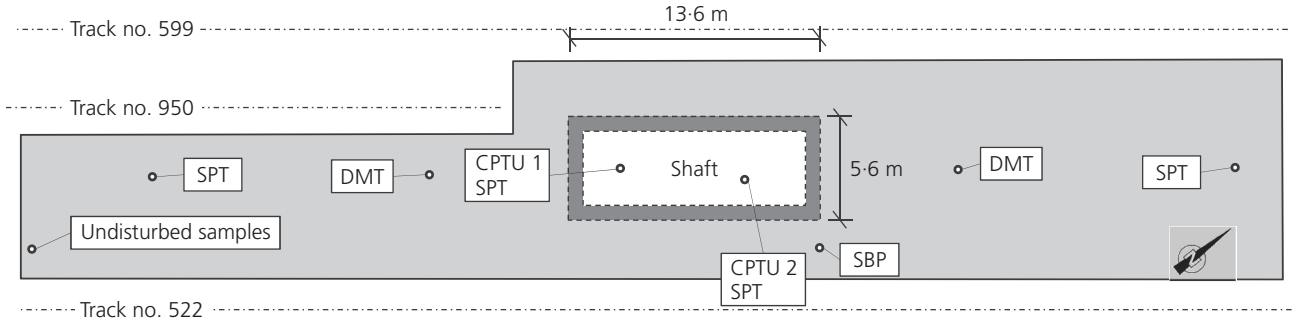

Figure 2. Plan view of test field, indicating position where in situ tests were carried out. The relative position of the tracks can also be observed

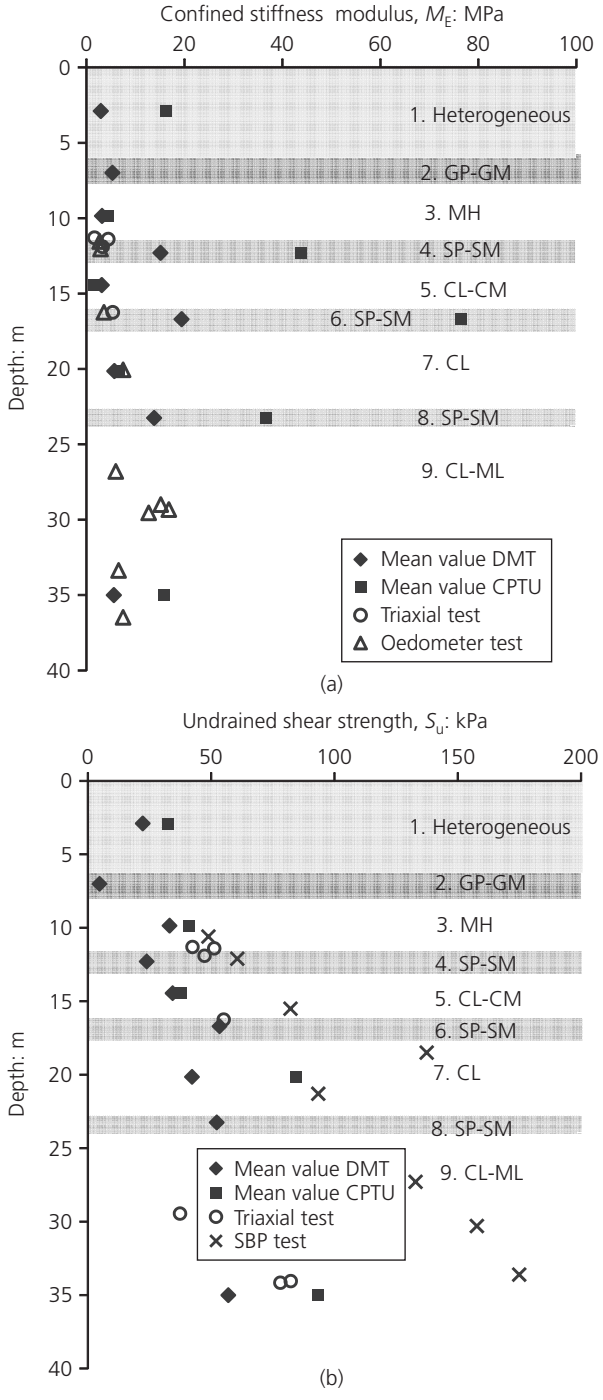

Figure 3. (a) Confined stiffness modulus as measured by different test methods. The soil type is described according to the USCS classification system. (b) Undrained shear strength as measured by different test methods. The soil type is described according to the USCS classification system

that a single soft layer and a single stiff layer are present throughout (equivalent soft and stiff layers). Statistical parameters of measured data for M_E of the stiff and soft layers, based on a lognormal distribution, are shown in Table 3. For M_E, with COV $> 0{\cdot}3$, a

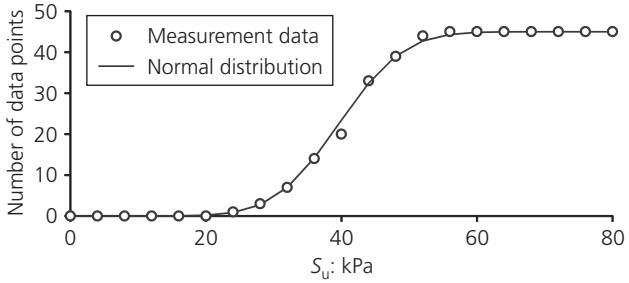

Figure 4. DMT tests, layers 5 and 7; cumulative normal distribution fitted to measured, undrained shear strength values

	λM_E: MPa	ζM_E: MPa	μM_E: MPa	$M_{E(50\%)}$: MPa
Soft layer (5 + 7)	1·5	0·8	5·8	4·3
Stiff layer (4 + 6 + 8)	2·8	0·5	18·2	16·4

Table 3. Measured logarithmic mean λ and standard deviation ζ of M_E for stiff and soft layers (DMT tests). The physical mean value μ and median are also shown

lognormal distribution is a better fit to the experimental stiffness data than a normal distribution, as was also found by Schneider and Schneider (2013). These distributions were used to obtain the properties of the geotechnical units shown in Tables 3 and 4.

In addition to its use in finding M_E assuming equivalent soft and stiff layers is also more convenient for back calculation and especially for the design of the future underground station, as CPTU tests in the station area and close surroundings illustrate that the genesis of the alluvium under the railway station has led to a high spatial variability of soft and stiff soil layers.

From the CPTU tests, the equivalent stiff layer near the test shaft is estimated to be 3·5 m for a total thickness of 12·3 m for unit D. The thickness of the soft layer is given by the difference between the total thickness of the layer D and that of the stiff layer.

The horizontal and vertical stiffness for layer D can be obtained from Equations 1 and 2

$$1.\quad M_{\mathrm{Eh,D}} = \frac{M_{\mathrm{E,a}} d_{\mathrm{a}} + M_{\mathrm{E,b}} d_{\mathrm{b}}}{d_{\mathrm{tot}}}$$

$$2.\quad M_{\mathrm{Ev,D}} = \frac{d_{\mathrm{tot}}}{\dfrac{d_{\mathrm{a}}}{M_{\mathrm{E,a}}} + \dfrac{d_{\mathrm{b}}}{M_{\mathrm{E,b}}}}$$

where a and b indicate the stiff and soft layer properties

Unit	μM_{Eh}: MPa	$M_{Eh(5\%)}$: MPa	$M_{Eh(95\%)}$: MPa	μS_u: kPa	$S_{u\,(5\%)}$: MPa	$S_{u\,(95\%)}$: MPa
A	3·9			23·4		
B	5·3			4·8		
C	3·3	2·3	4·5	33·7	24·0	43·5
D	9·4	4·2	17·8	39·6	27·2	52·0
E	7·2	1·8	17·9	59·1	33·0	85·2

Table 4. Mean values of measured horizontal stiffness and undrained shear strengths for the geotechnical units. The quantile values for the stiffness of unit D were derived from a Monte Carlo simulation with lognormal distribution of stiffness, as observed experimentally, and uniform distribution of thickness

subscripts, and M_{Eh} and M_{Ev} the horizontal and vertical confined stiffness moduli, d the thickness of the layers, d_{tot} the thickness of the geotechnical unit D.

Since the shaft walls are loaded and unloaded laterally, only the horizontal stiffness is further considered. The statistical properties of M_E are derived by using a Monte Carlo simulation. Figure 5 illustrates the lognormal distributions of M_E for both equivalent layers as well as for unit D as a whole.

3. Test shaft

3.1 Design and construction

Figure 6 shows the dimensions and the construction stages of the test shaft, as well as the main installed instrumentation. The final layout of the test shaft after construction can be observed in Figure 7. The shaft including the walls has a length of 13·6 m and a width of 5·6 m. The diaphragm walls, 80 cm thick and 24 m deep, consist of eight diaphragm wall barrettes. The corners of the diaphragm walls are formed by monolithic barrettes. The walls are supported by three steel struts and waler braces at depths of 4·1 m, 9·2 m and 12·2 m. The excavation took place in four stages. Jet grouting was carried out ahead of the excavation, with the purpose of supporting the excavation and sealing the shaft against groundwater. The jet grouting columns were approximately 2 m in diameter and were built with cement–air suspension (double fluid).

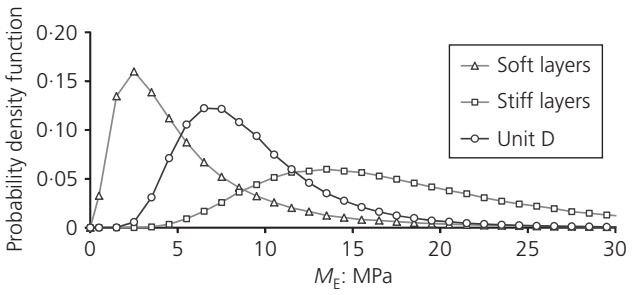

Figure 5. Probability density function for stiffness of layer D as predicted with Monte Carlo simulation

The adopted jet grouting pressure, between 40 and 45 MPa, was on the upper boundary of typical values that can be found in literature (Croce *et al.*, 2014). Other construction parameters were in the mid-ranges of literature values for double fluid jet grouting.

During the jet grouting, crack openings with a width of approximately 2 cm were observed at the corners of the shaft. The walls were pushed into the soil, with a maximum horizontal displacement of 13 cm at −12 m depth. The crack openings partly closed during excavation. The strut forces that were measured by strain gauges during excavation were far greater than those predicted by using active or even at-rest earth pressure, and therefore an extra four struts were added in the last two excavation stages. All struts were of type HEB300 and were equipped with strain gauges. The forces in the lowest strut continued to increase after the final excavation was terminated.

3.2 Instrumentation

Several measuring devices were installed in the shaft and the surrounding soil (Figure 6). Slope indicators were built inside the walls of the shaft and in the soil at a distance of 1·5 m from the wall, in line with the struts. In pipes of the slope indicators, inclinodeformeter (IDM) measurements were also carried out (Schwager, 2013). The analysis of IDM test results allows changes in the earth soil pressure or the soil stiffness to be estimated by making very precise measurements of the induced change in the shape of the slope indicator pipe. The forces in the struts during excavation were measured with strain gauges.

4. Analysis

4.1 General problem and forensic analysis

In contrast to reports in the literature (Wang *et al.*, 1999), the earth pressure generated by the jetting works did not dissipate over time. During excavation, no changes were observed in the soil matrix above the slab. Standard penetration tests (SPTs) carried out inside

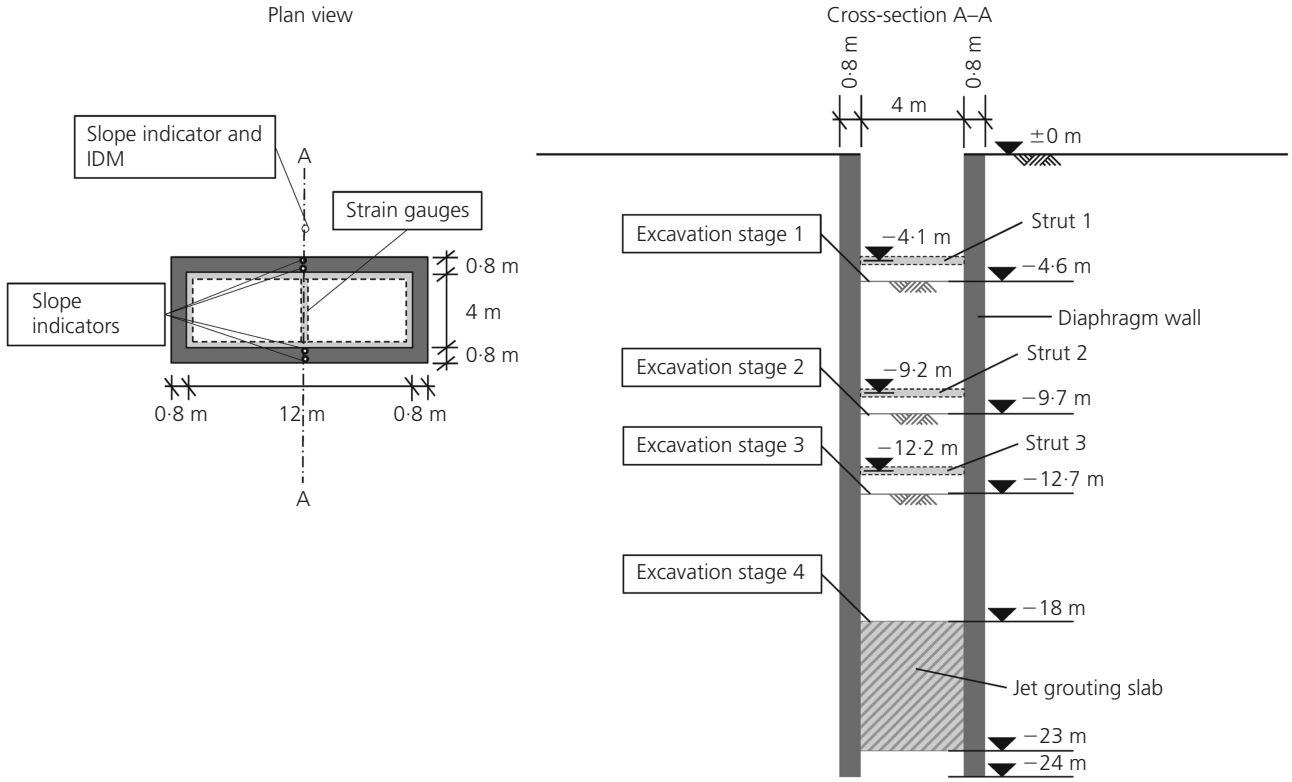

Figure 6. Plan view and cross-section of the test shaft indicating depth of struts and excavation stages, as well as installed instrumentation

the shaft before and after the jet grouting showed no significant changes in the soil properties above the slab.

Since the deformation of the shaft was permanent, it is likely that the jet grouting mixture replaced material from layer D that was squeezed out upwards and therefore inflated the shaft (Figure 8). If the deformation was caused only by the generated pressure, elastic rebound of the shaft would have taken place by the end of the jet grouting process, instead of later, during the excavation. The IDM measurements also confirm this hypothesis: the measured change in the earth pressure did not dissipate after the jet grouting process had ended (Schwager, 2013).

This issue represented a severe problem for the construction of the shaft. A useful feature, however, is that the shaft can be interpreted as an in situ test device.

4.2 Finite-element model and analysis

In order to investigate the observed phenomena, a three-dimensional (3D) finite-element analysis was carried out with the finite-element program Plaxis3D (Brinkgreve *et al.*, 2013). Within this analysis it was possible to back-calculate soil parameters based on measured forces, stresses and displacements of the shaft and of the soil.

The finite-element model is symmetric and represents one-quarter of the shaft. Its dimensions are $50 \times 50 \times 50$ m with 33 620 tetrahedral (soil and concrete) and beam (struts and walers) elements and 51 237 nodes (Figure 9). The axis of symmetry is at the centre of the shaft.

The strut sections and lengths are half of the real dimensions, owing to the symmetry of the model. Additionally, the struts are fixed horizontally at the halfway point (model edge).

The constitutive model adopted for modelling the behaviour of the soil, jet grout and concrete is an elasto-perfectly plastic model with Tresca's failure criterion. The strut and waler brace materials are modelled as purely elastic. The analysis was carried out using total stresses and undrained strength and stiffness parameters (C Method in Plaxis3D).

The following construction stages were simulated

(*a*) gravity (only soil materials, no structures modelled)
(*b*) building of the diaphragm wall (wall elements: soil material replaced with concrete)
(*c*) jet grouting (equivalent pressure applied)
(*d*) excavation stage 1 (jet grouting slab elements: soil material replaced with grout, equivalent earth pressure removed in excavated soil elements)
(*e*) installation of struts and waler braces

Figure 7. Construction of test shaft on platform between rail tracks

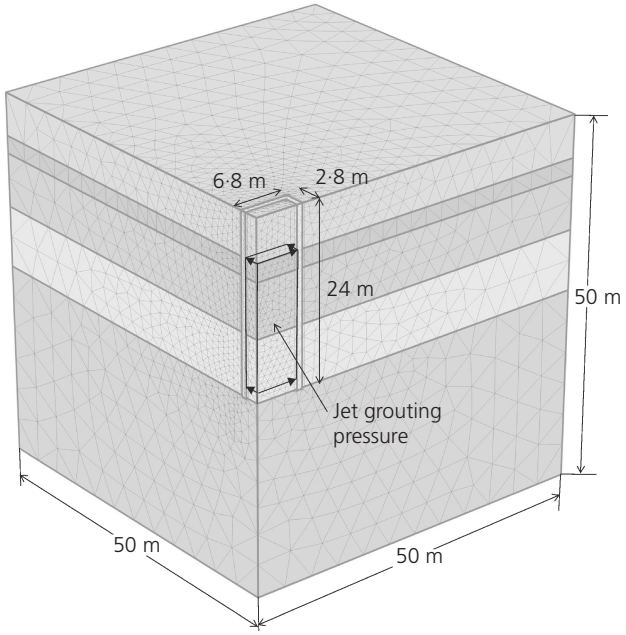

Figure 9. Main dimensions of the three-dimensional symmetric finite-element model adopted for the simulation

(*f*) excavation stage 2 (equivalent earth pressure removed in excavated soil elements)
(*g*) installation of struts and waler braces
(*h*) excavation stage 3 (equivalent earth pressure removed in excavated soil elements)
(*i*) installation of struts and waler braces

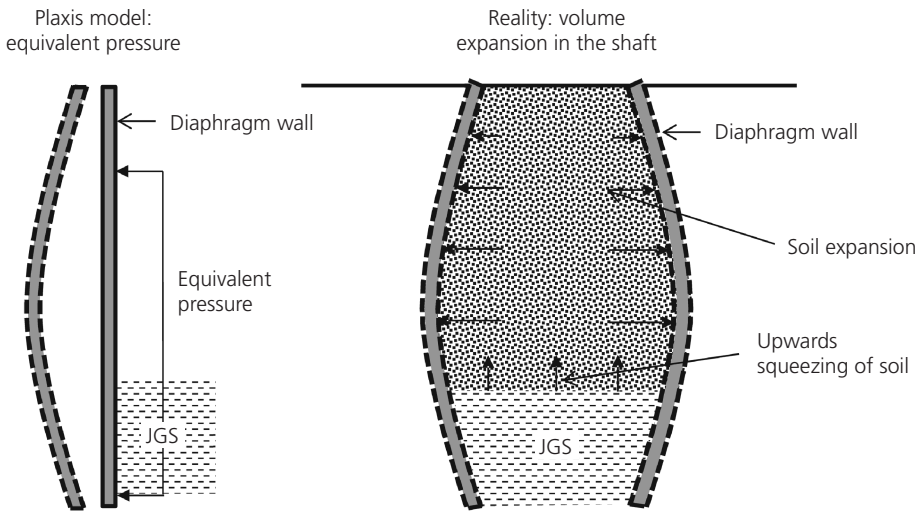

Figure 8. Jet grouting increased volume inside shaft and pushed diaphragm walls into the surrounding soil. In the PLAXIS model this was modelled with an equivalent pressure

(*j*) excavation stage 4 (equivalent earth pressure removed in excavated soil elements and in the jet grouting slab).

The construction of the jet grout columns was modelled as additional pressure acting on the wall inside the shaft (Figures 8 and 9), which was then set stepwise to zero during excavation as the corresponding volume was removed.

The simple linear elasto-plastic soil model was adopted in order to reduce the number of parameters to be obtained in the back-calculation, therefore avoiding the formulation of an ill-posed inverse problem. It uses unloading–reloading stiffness and undrained shear strength, and it does not take into account strain hardening, pressure dependency and small strain stiffness (Puzrin, 2012). Nevertheless, when incorporated into the boundary value problem it was capable of reproducing the behaviour of the shaft during jet grouting and excavation quite realistically, in particular the loading–unloading behaviour.

4.3 Back-calculation

The construction of the shaft can be considered as a continuum mechanics problem. The displacements were measured by the slope indicators in the wall and in the soil, the stresses by the IDM, and the forces by the strain gauges in the struts. During jet grouting (loading) the increase in the earth pressure could be obtained directly from the IDM measurements. During excavation (unloading), the total earth pressure could be indirectly obtained from the forces measured in the struts, provided that the area where the equivalent pressure was applied was known: this could be determined by observing the shape of the diaphragm wall deformation. Knowing the stress and the strain field also allowed the soil stiffness properties to be obtained.

The back-calculation was carried out by matching the calculated and measured displacements of the soil and the wall (Figures 10(a) and 10(b)) as well as the calculated and measured forces in the struts (Figures 11(a) and 11(b)). The parameters obtained were validated by comparing the calculated and measured (IDM) earth pressures, as shown in Figure 12. The main unknowns were the undrained shear strength and stiffness (primary loading) of the layers, as well as the jetting pressure and the surface area of the compression zone. The Poisson ratio was chosen to be equal to 0·2 for all layers, but it was found that its value did not affect the calculation results.

The following parameters were fixed in the back calculation.

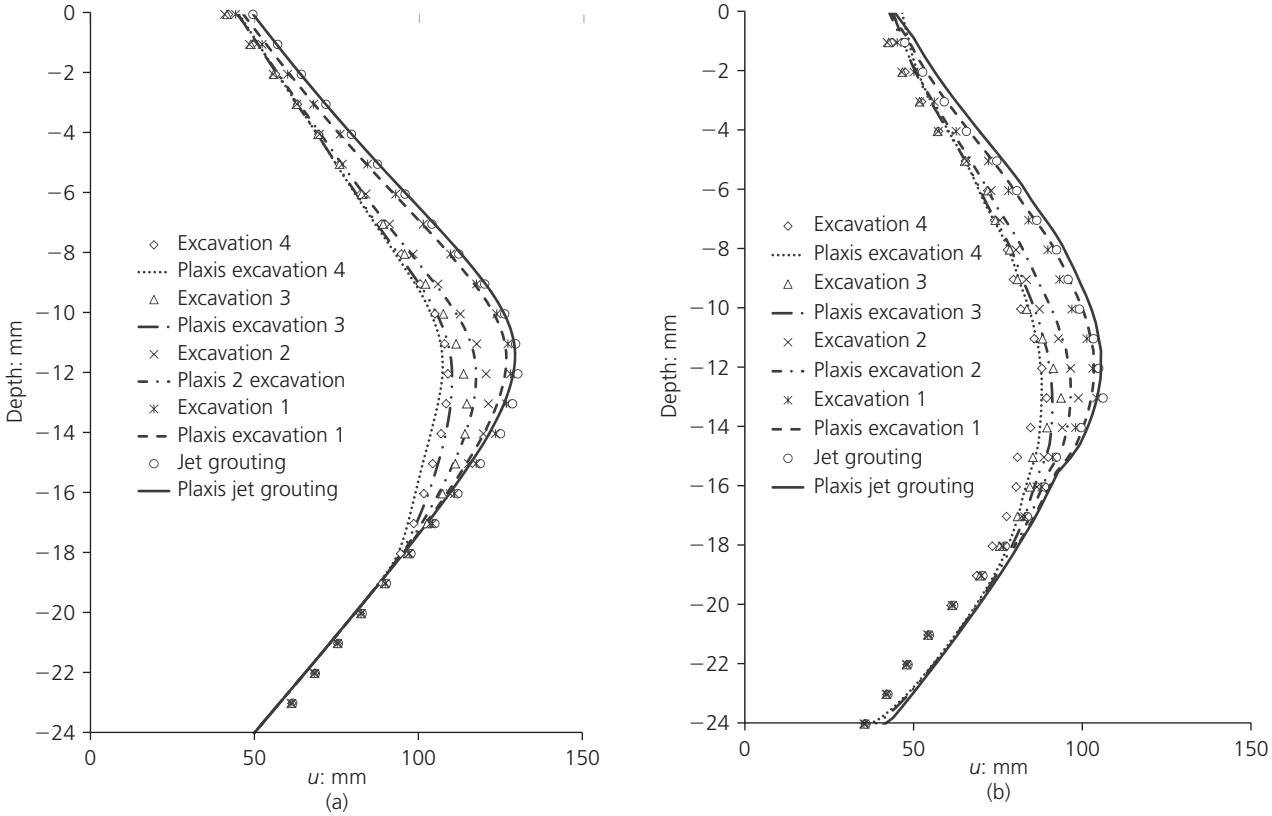

Figure 10. (a) Diaphragm wall displacements measured by built-in slope indicators (dots) and predicted by finite-element model (lines). (b) Soil horizontal displacements measured by built-in slope indicators (dots) and predicted by finite-element model (lines)

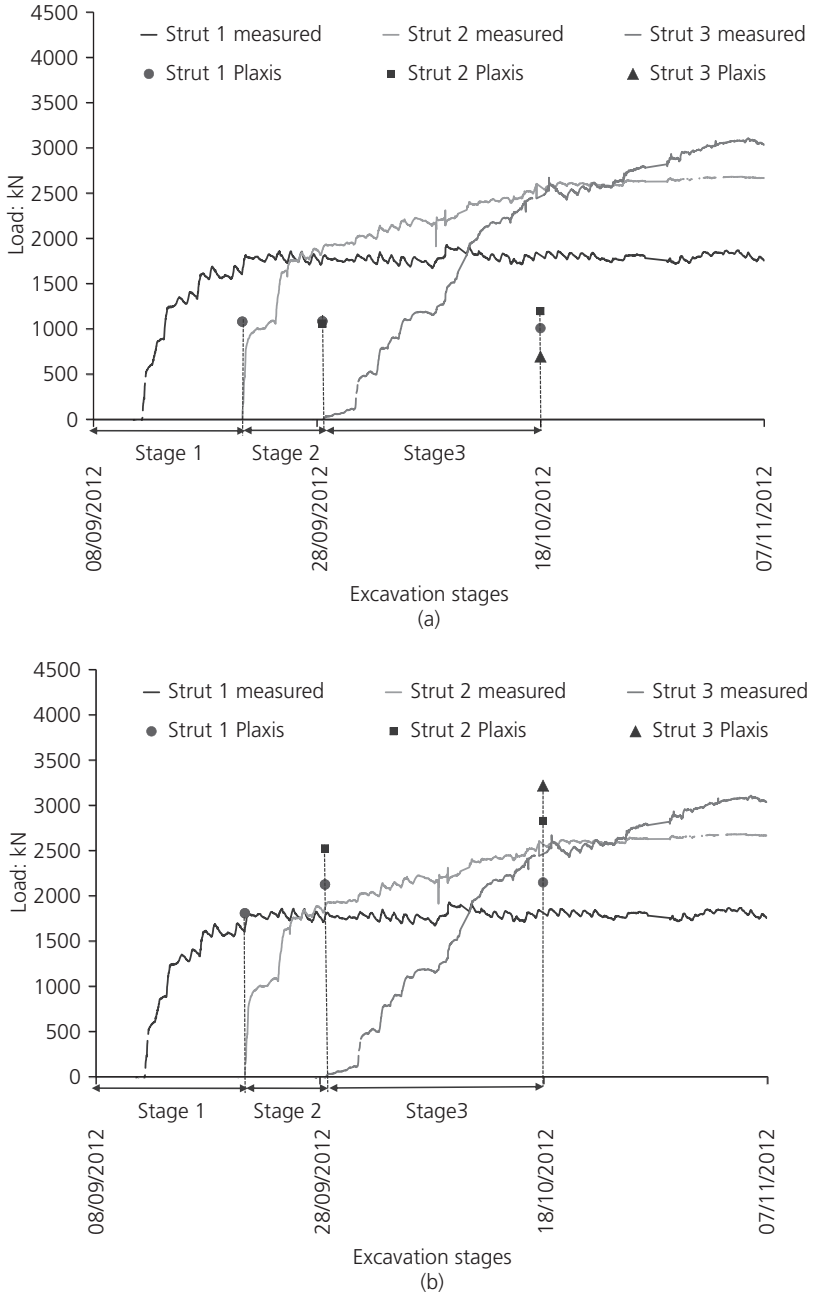

Figure 11. (a) Strut forces predicted by finite-element simulation without taking into account the jetting pressure (dots), and strut forces measured by strain gauge (lines). (b) Strut forces predicted by finite-element simulation (dots), and strut forces measured by strain gauge (lines)

- The tensile strength of the wall was set equal to the tensile strength of concrete, owing to the lack of horizontal steel reinforcement between the elements of the diaphragm walls.
- The concrete shear (compressive) strength was set to infinity, since no shear-failure-related cracks have been observed in the walls.
- The elastic modulus E of the concrete was chosen according to its technical specifications.
- The concrete–soil interface strength was considered to be two-thirds that of the surrounding soil based on standard geotechnical practice assumptions.
- The stiffness of the struts was calculated from the measured forces and the wall displacements. The reason for the reduction in the strut stiffness lay in the (soft) grout that was placed behind the waler braces in order to obtain a continuous smooth contact. In order to reduce the strut stiffness in the model during the simulated excavation, the section area A^* was reduced, rather than the elastic modulus

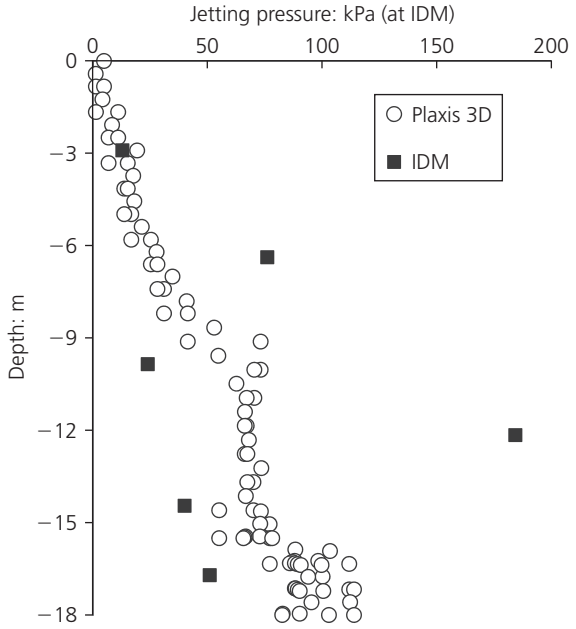

Figure 12. Earth pressure decrease in the soft layers as measured by IDM and calculated with the finite-element model

E. In this way the bending stiffness *EI* of the struts is calculated correctly by the program, since the moment of inertia *I* is an independent input parameter (Table 5).

- Jet grout stiffness and strength were measured in uniaxial loading tests. The same constitutive model as for the soil was adopted.

In the process of the back-calculation, the sensitivity of the wall displacements to changes in soil properties and jet grouting pressure was studied. Generally, the wall and soil displacements appeared to be sensitive to changes in the jet grouting equivalent pressure and its area of application. This is due to the yielding of the soil and structure (after the jet grouting equivalent pressure had reached approximately 200–250 kPa). Once the soil had yielded, variation in the jet grouting pressure had a moderate influence on the elastic rebound of the wall during the excavation and a greater influence on the strut forces, since (as was also measured in situ) the pressures did not dissipate and were transferred to the struts during excavation. The undrained shear strength of the soil had a strong influence on the deformations but a low impact on the strut forces, which are more strongly influenced by the elastic properties. On the other hand, the soil shear strength had a strong influence on the wall and soil deformation, owing to the yielding that took place, whereas the elastic rebound was mainly driven by the elastic (reversible) properties of the soil.

Material	Elastic modulus, *E*: GPa	Uniaxial compressive strength, σ_c: kPa	Tensile strength, σ_t: kPa	Area (section), A^*:[b] mm^2
Concrete	30	∞	3700	—
Grout	6	5600	0	—
Strut Ia		∞	∞	1500
Strut Ib[a]	210	∞	∞	7000
Strut IIa	210	∞	∞	2500
Strut IIb[a]	210	∞	∞	7000
Strut IIIa	210	∞	∞	5500
Strut IIIb[a]	210	∞	∞	7000

[a] The strut stiffness is adjusted to the real value after the next excavation step.
[b] A^* was reduced instead of *E* in order not to affect the bending stiffness of the struts. In the model, the strut thickness is half the real thickness.

Table 5. Properties of the structural elements

4.4 Results

Figures 10(a) and 10(b) show the wall and the soil displacement during the jet grouting process and all excavation stages measured with the embedded slope indicators (points). They also show the values obtained from the finite-element model (lines), once the jet grouting equivalent pressure was taken into account. The location of the point of maximum displacement and the shape of the deformed wall depend mainly on the relative stiffness of the soil as compared to that of the diaphragm wall, and on the jetting pressure. It was found that a pressure of at least 360 kPa from −23 m up to −5·8 m (17·2 m), which corresponds to the top of layer B, was necessary to push the diaphragm wall into the soil by the observed value of 130 mm (maximum). The maximum displacement was measured at −12 m, well above the top of the jet grouting slab, which was cast between −18 m and −23 m.

Figure 11(a) shows the forces in the struts in the shaft as they were predicted without taking into account the effects of jet grouting on the shaft, and compares these with the measured forces. The forces measured in the struts were extremely high, up to 2·5 times those predicted by the model without the pre-stress due to jet grouting. However, Figure 11(b) shows that once the jet grouting equivalent pressure is applied, the forces predicted by the finite-element model match those measured by the strain gauges quite well.

Figure 12 shows the earth pressure increase predicted by the finite-element model and measured by the IDM. The IDM results show higher values in the stiff layers and lower pressure values for the soft layers (see also Schwager, 2013). The calculated pressures fall within the IDM measured range. This makes sense, since the finite-element model considers equivalent properties for a layer (D) made up of stiff and soft material. Generally, the calculated pressure values are closer to the lower measured values. As the thickness of the stiff layers is lower than those of the soft layers, their contribution to the thickness-weighted average pressure for the equivalent layer (D) is less significant.

4.5 Discussion

Table 6 compares the measured soil properties with the results from the inverse analysis. It can be seen that the stiffness parameters from the inverse analysis are comparable to those obtained from the statistical analyses of DMT measurements. The stiffness and undrained shear strength of layers D and E matched well with the mean values measured by the in situ tests. The undrained shear strengths of layer A from the back-calculation were much lower. The reason is that much of layer A is a narrow embankment; therefore its contribution for the first 1–2 m is very low. In the finite-element model, this was modelled as a continuous layer. The back-calculated undrained shear strength of layer B is double that measured. One possible explanation is that layer B is made of gravel, so that the undrained analysis is not entirely correct. The undrained strength of layer C is slightly lower than the lower bound of the values measured with the in situ tests.

Matching of the calculated and measured wall and soil displacements also presented some discrepancies (Figures 10(a) and 10(b)). The calculated rebound of the wall from the second excavation stage was slightly larger than measured, while the calculated soil displacement due to jet grouting was slightly larger than that measured in the deeper layers. These small discrepancies cannot be avoided, considering the many simplifications adopted, as listed below.

- The effect of the mortar between strut, walers and diaphragm wall was modelled in a simplified manner as reduced strut stiffness.
- Many different layers have been homogenised into one single layer in the model.
- Simplified constitutive models were adopted for concrete and the soil.
- The diaphragm wall has joints that can rotate around a vertical axis, and these were not taken into account in the finite-element model.
- The measurement accuracy and precision have their limits.

Nevertheless the analysis allowed an understanding of the shaft behaviour and provided a reasonably good match between measured and calculated values.

Geotechnical unit		A	B	C	D	E
$M_{Eh(5\%)}$	MPa			2·3	4·2	1·8
μM_E	MPa	3·9	5·3	3·3	9·4	7·2
$M_{Eh(95\%)}$	MPa			4·5	17·8	17·9
M_E BC	MPa	4·8	3·4	4·5	8	5·6
$S_{u\,(5\%)}$	kPa			24·0	27·2	33·0
μS_u	kPa	23·4	4·8	33·7	39·6	59·1
$S_{u\,(95\%)}$	kPa			43·5	52·0	85·2
S_u BC	kPa	5	10	20	40	50

Table 6. Properties of geotechnical units from probabilistic analyses and back-calculation (BC)

The calculated forces in the struts matched the measured values reasonably well (Figure 11(b)). The finite-element model slightly over-predicted the force in the first strut. This is because the 4-m-deep guide walls adopted for the construction of the diaphragm walls were not taken into account in the finite-element model, and also because the shaft was built on a narrow platform (see Figure 7), which was approximately 1·5 m higher than the track level.

In the original design of the shaft, many conservative assumptions and a risk management strategy coupled with a precise observational method were adopted. In this way it was possible to ensure the safety of the excavation during the process: extra struts were added as soon as the measured forces reached the alarm values.

5. Summary and conclusion

The construction techniques for a planned large underground project in the city of Lucerne (Switzerland) have been tested by excavating, building and instrumenting a deep test shaft, preceded by many in situ and laboratory tests to characterise the soil properties. An extensive analysis has been carried out in order to discover the reasons for the higher than expected strut forces measured during the braced excavation. The analysis was supported by the large amount of data (including soil displacements, soil pressures and strut forces) measured during the excavation.

The main results of the analysis are summarised below.

(*a*) The equivalent pressure inside the shaft due to jet grouting was about 360 kPa over a height range of 17·2 m from the bottom of the slab at −23 m, to −5·8 m (the measured thickness of the slab is 5 m, from −23 m to −18 m).
(*b*) The strut forces reacted not only to existing earth pressure but also to the pre-stressing of the soil and of the structure caused by the jet grouting: the measured forces were 2·5 times those predicted by the model without taking into account the jet grouting equivalent pressure.
(*c*) The soil parameters obtained from the back-analysis of the shaft measurements compare reasonably well with those obtained from the statistical analysis of DMT test results.

The results of the analysis showed that jet grouting in soft soils can pre-stress soil-embedded structures such as diaphragm walls. Moreover, these additional stresses have to be supported by the retaining system if an excavation is carried out inside the same walls. Of course, these problems could be avoided by using appropriate jet grouting techniques allowing for elastic rebound before installing the retaining system; nevertheless, the risk could be present and should not be underestimated.

The forces on struts can exceed the design loads and bring the

retaining wall system to failure. Therefore the strut forces should be measured and, if needed, additional struts should immediately be installed during the excavation, in order to prevent catastrophic collapse. Alternatively a compression zone in the struts, similar to the measure adopted for lining systems in squeezing rock in tunnelling engineering, could be considered. In this way the elastic rebound of the walls could take place, and the struts would be loaded only with the at-rest or active earth pressure. Particular attention should be paid to soft soils, where the displacement due to soil relaxation after the jet grouting process can be very large and could therefore require a more flexible retaining system. Another option could be to cast the jet grouting slab before the diaphragm walls are built. In this case the construction of the walls would be more expensive, owing to necessary trenching for the jet grout columns.

Acknowledgements

The authors would like to acknowledge the Swiss Federal Railways and the Canton Lucerne for approving and supporting the realisation of the test shaft, which is an important component of the design process for the structures of the future underground station. Jason Messerli, Bernhard Trommer and Martin Bosshard (Basler & Hofmann) are acknowledged for their effort in the project design, technical site supervision and project management of the test shaft as well as their valuable comments and input to the paper.

The authors are also grateful to the group of Professor Springman (ETH Zürich), in particular Ralf Herzog, for carrying out the laboratory tests on the soil samples. Markus Schwager from ETH is acknowledged for the IDM measurement results which were crucial for the validation of the analysis carried out here.

The authors would like to thank Mark Schneider (Basler & Hofmann) for fruitful discussions and input to this study.

REFERENCES

Brinkgreve RBJ, Engin E and Swolfs WM (2013) *Plaxis3D User Manual*. Plaxis, Delft, the Netherlands.

Croce P, Flora A and Modoni G (2014) *Jet Grouting: Technology, Design and Control*. CRC Press, Boca Reton, FL, USA.

IG TiBLU (2013) *Geotechnische Vorversuche – Dokumentation der Ergebnisse*. Busler A Hofmann AG, Zurich, Switzerland, Report B 5018-016, Rev. 0, p. 1222 (in German).

Keller B (2011) *Geologie, Hydrogeologie und Geotechnik. Tiefbahnhof Luzern Grundlagen für Vorprojekt*. Keller + Lovenz AG, Kriers, Switzerland, Report 2A1, p. 47 (in German).

Poh TY and Wong IH (2001) A field trial of jet-grouting in marine clay. *Canadian Geotechnical Journal* **38(2)**: 338–348.

Puzrin AM, Alonso EE and Pinyol NM (2010) *Geomechanics of Failures*. Springer-Verlag, Berlin, Germany.

Puzrin AM (2012) *Constitutive Modelling in Geomechanics – Introduction*. Springer-Verlag, Berlin, Germany.

Schneider HR and Schneider MA (2013) *Dealing with Uncertainties in EC7 with Emphasis on Determination of Characteristic Soil Properties, Modern Geotechnical Design Codes of Practice*. IOS Press, Amsterdam, the Netherlands.

Schwager MV (2013) *Development, Analysis and Applications of an Inclinodeformeter Device for Earth Pressure Measurements*. PhD thesis, ETH, Zürich, Switzerland.

Wang JG, Oh B, Lim SW and Kumar GS (1999) Effect of different jet-grouting installations on neighboring structures. In *Proceedings of the 5th International Symposium on Field Measurements in Geomechanics – FMGM99, Singapore* (Leung CF, Tan SA and Phoon KK (eds)). Balkema, Rotterdam, the Netherlands, pp. 511–516.

Wang ZF, Shen SL, Ho EC and Kim YH (2013) Investigation of field-installation effects of horizontal twin-jet-grouting in Shanghai soft soil deposits. *Canadian Geotechnical Journal* **50(3)**: 288–297.